Energy Reports 8 (2022) 6901–6913

Contents lists available at ScienceDirect

Energy Reports

journal homepage: www.elsevier.com/locate/egyr

Research paper

The main controlling factors on shale gas occurrence characteristics in deep and high-over mature shales: A case study of Silurian Longmaxi Formation in the Sichuan Basin, southern China

Min Li [a,b], Xiongqi Pang [a,b,*], Liang Xiong [c], Tao Hu [a,b], Di Chen [a,b], Zhen Zhao [a,b], Shasha Hui [a,b], Yang Liu [a,b], Siyu Zhang [a,b]

[a] State Key Laboratory of Petroleum Resources and Prospecting, China University of Petroleum (Beijing), Beijing 102249, China
[b] College of Geosciences, China University of Petroleum (Beijing), Beijing 102249, China
[c] Research Institute of Exploration and Development, SINOPEC Southwest Branch Company, Chengdu 610041, China

ARTICLE INFO

Article history:
Received 19 January 2022
Received in revised form 26 April 2022
Accepted 11 May 2022
Available online xxxx

Keywords:
Deep shale
Adsorbed gas
Free gas
Gas content
High pressure
Pore structure

ABSTRACT

Deep shales refer to the shales with buried depth greater than 3500 m. Yields of shale gases depend on the form of their occurrence at the depth, but the major controlling factors on shale gas occurrence state in deep high-over mature shales are poorly understood. Using the Longmaxi Formation as an example, the shale gas occurrence characteristics of deep high-over mature shales were quantitatively characterized, and the effects of temperature, pressure, pore structure, and organic matter abundance on the occurrence characteristics of shale gas were studied by using the control variable method. The results show that the Longmaxi shale is mainly organic-rich argillaceous shale, with an average porosity of 7.54%. The pore volumes are mainly contributed by mesopores, whereas the total specific surface areas are primarily by micropores. The Longmaxi shale has high gas contents, with total gas contents of 3.82∼7.89 m^3/t rock, in which the proportion of free gas varies from 71% to 83%, with an average of 77%. The high proportion of free gas depends on the particular geological conditions in the Longmaxi Formation. High temperature is not conducive to shale gas storage, and its negative effect on adsorbed gas is greater than that on free gas. High pressure is beneficial to shale gas storage, and its positive influence on free gas is greater than that on adsorbed gas. The large pore volume dominated by mesopores provides sufficient storage place for free gas. High organic matter content is beneficial for shale gas enrichment but reduce the proportion of free gas. In conclusion, high pressure and large pore volume are the major factors for the high proportion of free gas.

1. Introduction

The potential of shale gas resources is great globally (Hou et al., 2021; Hu et al., 2021a). At present, the exploration and development technology of shale gas is becoming more and more perfect (Gou et al., 2021). Countries represented by the United States, Canada and China have taken the lead in realizing the commercial production of shale gas, especially shallow shale gas. Recently, petroleum geologists begin to focus on deep shale gas which is stored in high temperature and high pressure formations with buried depth greater than 3500 m and is generally in high-over mature stage. Practice shows that deep shale gas has great exploration potential. For example, the Wufeng–Longmaxi Formation in the southern Sichuan Basin is the main battlefield for commercial development of shale gas in China. Its deep shale gas geological resources amount to 16 trillion cubic meters, accounting for approximately 84% of the total shale gas geological resources (Ma et al., 2021). PetroChina and Sinopec explored and developed deep shale gas in the Wufeng–Longmaxi Formation in Luzhou, Weiyuan, and Dingshan areas in the Sichuan Basin and drilled several high-yield shale gas wells. For example, well L203 in southern Sichuan obtained a shale gas test production of 138 × 10^4 m^3/d, and the shale gas test output of well DY4 in southeastern Sichuan is 20.56 × 10^4 m^3/d, which strongly confirms the considerable resource potential of deep shale gas (Yang et al., 2021).

Shale gas is stored in micro and nano pores of shale in various occurrence states such as free gas, adsorbed gas, and dissolved gas, and dissolved gas can be negligible due to low content (Chen et al., 2019a; Etminan et al., 2014; Guo et al., 2020; Hao et al., 2013; Zhu et al., 2020). The relative content of adsorbed gas and free gas affects shale gas development because free gas

* Correspondence to: No. 18 Fuxue Road, Changping District, Beijing, 102249, China.
E-mail address: pangxq@cup.edu.cn (X. Pang).

https://doi.org/10.1016/j.egyr.2022.05.037

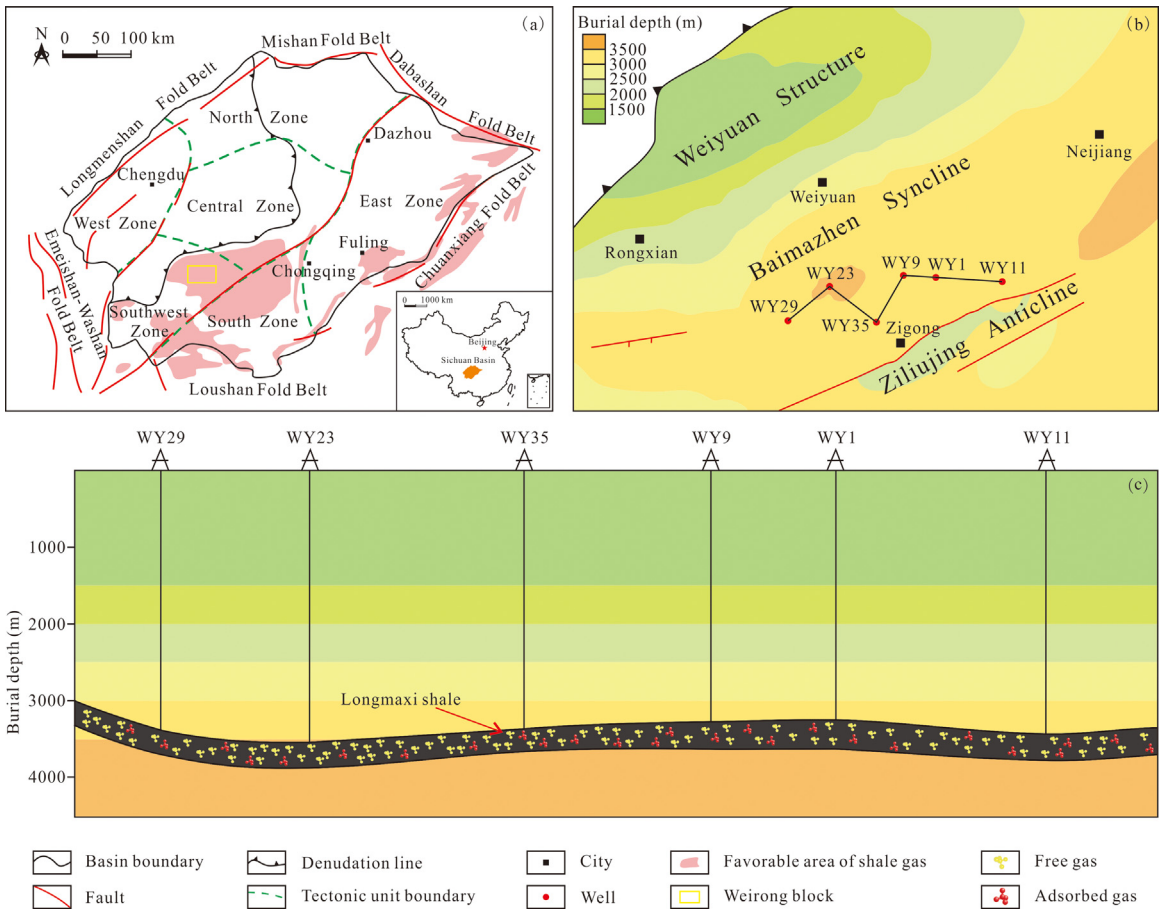

Fig. 1. (a) is the sketch map showing the structural outline of the Sichuan Basin and the location of the Weirong block (modified after Nie et al. (2021)); (b) is the regional map of the Weirong block (modified after Tang et al. (2021) and Xiong (2019)); (c) shows the profile of Longmaxi shale (modified after Tang et al. (2021) and Xiong (2019)).

determines the initial production capacity while adsorbed gas determines the production longevity of shale gas well (Ji et al., 2012). Research shows that the relative content of adsorbed gas and free gas varies significantly in shales with different burial depths and maturities (Li et al., 2018b). For example, the low mature Antrim Shale with burial depth less than 1000 m in the San Juan Basin has adsorbed and free gas contents of 70% and 30%, the adsorbed and free gas contents of medium-high mature Bartnett Shale with burial depth of 1000∼2500 m in the Fort Worth Basin are 60% and 40%, the over mature Horn River Shale with burial depth of 2500∼3000 m in the Anadarko Basin has adsorbed and free gas contents of 34% and 66%, and the proportions of adsorbed and free gas of the over mature Haynesville Shale with burial depth of 3350∼4000 m in the North Louisiana Basin are 20% and 80% (Curtis, 2002; Montgomery et al., 2005; Zou et al., 2020). It is found that free gas is more enriched than adsorbed gas in shale with large buried depth and high maturity. However, the occurrence characteristics of shale gas and its main controlling factors in deep high-over mature shale have not been extensively discussed. This paper aims to quantitatively characterize the shale gas occurrence characteristic of deep high-over mature shale, taking the Silurian Longmaxi Formation in the Weirong block, southern Sichuan as an example, and discusses the main influencing factors of shale gas occurrence. The research results are expected to provide theoretical guidance for the prediction of deep shale gas “sweet spot” in the Sichuan Basin and other areas in the world.

2. Geological setting

The Sichuan Basin is a superimposed petroliferous basin in southwestern China, which evolved from a passive continental margin to a foreland basin in the late Triassic (Dai et al., 2014; Nie et al., 2020). The Sichuan Basin is divided into six tectonic units, which are the north low-gentle structural belt, east high-steep structural belt, west low-steep structural belt, south low-lying structural belt, southwest low-fold structural belt, and central gentle structural belt, respectively (Nie et al., 2021; Yang et al., 2016a; Fig. 1a). The Weirong block structurally belongs to the southwest low-fold structural belt. It is located in the Baimazhen syncline between the southeast wing of the Weiyuan structure and the Ziliujing anticline (Cao et al., 2020; Fig. 1b). Controlled by the Weiyuan large dome anticline, the structure is gentle (Zhou et al., 2014).

The Longmaxi Formation, especially the lower Longmaxi, is the important shale gas production layer for the Weirong block. During the Early Silurian, the global transgression occurred, and the Longmaxi Formation was deposited in deep-water shelf to shallow-water shelf environments (Cao et al., 2015; Ma et al., 2016). The Longmaxi Formation can be approximately divided into two members according to lithology. The lower Longmaxi member is mainly black carbonaceous shale with abundant graptolite and radiolarian. The lithology of the upper Longmaxi member mainly consists of calcareous silty shale and gradually changes upward into dark gray mudstone. The burial depth of the Longmaxi Formation in the study area is generally greater than 3500 m (Fig. 1c). The values of equivalent reflectance of

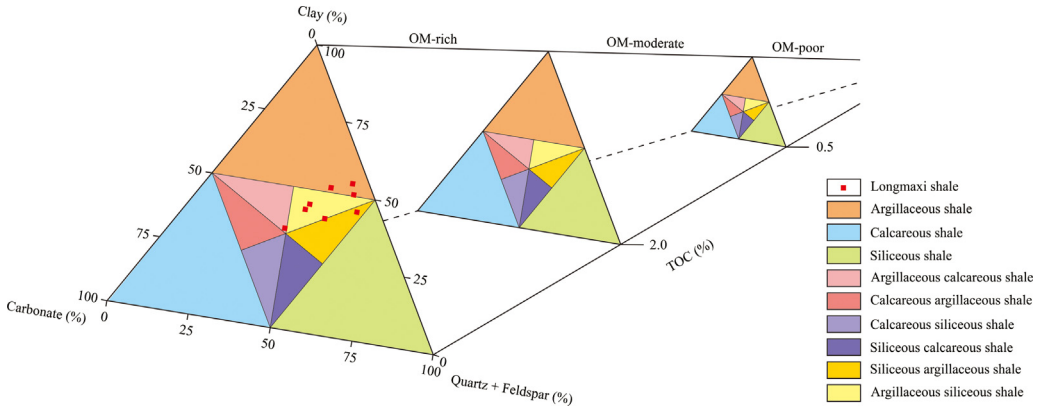

Fig. 2. Lithofacies classification of the Longmaxi shale samples in the Weirong block, Sichuan Basin (modified after Yuan et al., 2021).

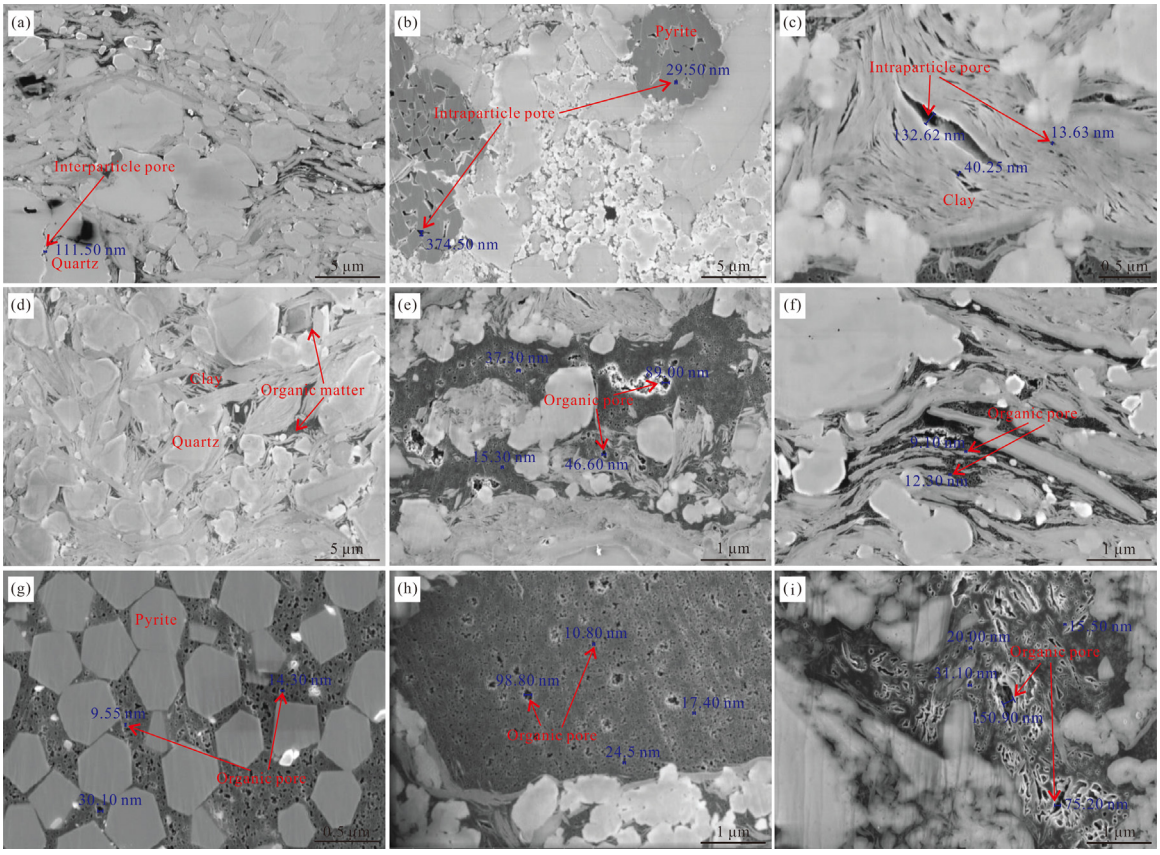

Fig. 3. Pores in the Longmaxi shale samples in the Weirong block, Sichuan Basin. (a) Interparticle pores between quartz grains; (b) Intercrystalline pores within pyrite frambodies; (c) Intraplatelet pores within clay aggregates; (d) Organic matter filled pore space between quartz and clay minerals; (e) Mesopores and micropores developed in organic matter filled between mineral grains; (f) Micropores developed in organic matter filled in clay aggregates; (g) Micropores developed in organic matter filled in pyrite frambodies; (h) Circular pores in organic matter; (i) Elongated pores in organic matter.

the Longmaxi shale are mainly in the range of 1.95%∼3.20%, indicating that the Longmaxi shale of the study area is a critical target reservoir for shale gas exploration and development.

3. Material and methods

3.1. Samples and experiments

The Longmaxi shale samples were obtained from the WY23 well at a depth of 3815∼3841 m.

Samples were crushed to powders to 0.2 mm sieve. The powder of 0.1 g was treated with sufficient diluted hydrochloric acid to remove carbonates and then was washed and dried. Then the total organic carbon (TOC) content was measured by a LECO CS400 carbon sulfur analyzer.

Sample powders with the grain size of 40 μm were prepared for X-ray Diffraction (XRD) analysis, performed on a D/max-2500 diffractometer using Co Kα radiation. The diffracted beams scanned in the sample powders at a rate of 2°(2θ)/min in the range of 3∼85°(2θ) (Hu et al., 2021b). The relative mineral percentages were determined by estimating the area of the specified peaks in the spectrogram (Tian et al., 2016).

The samples were prepared as cylindrical plugs with 2.54 cm in diameter and 2.54 cm in length. The bulk volumes of these plug

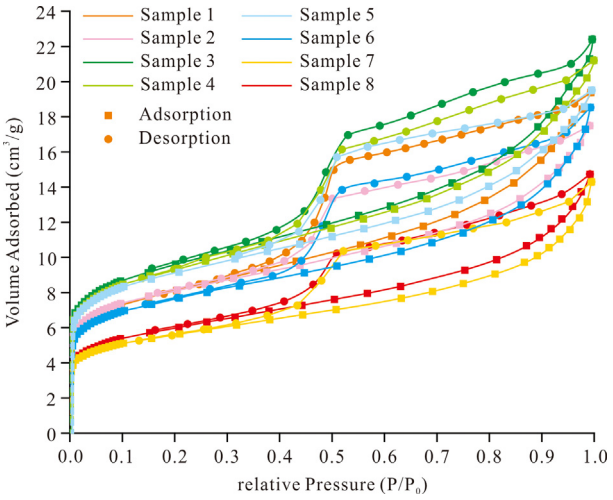

Fig. 4. Nitrogen adsorption and desorption isotherms for the Longmaxi shale samples in the Weirong block, Sichuan Basin.

samples were measured by the Archimedes method (Gasparik et al., 2014). After that, these plug samples were crushed into powders with the grain size of 0.25 mm, which was weighed and used for determining the grain volume with Boyle's law porosimeter. Then the grain density and porosity were obtained from the grain volume, the grain mass, and the bulk volume (Hu et al., 2019).

Water saturation was measured by the retort method (Li et al., 2021a). 100 g crushed samples with a diameter of 6.4 mm were put into a sample cup in the insulated oven. The temperature of the oven was set at 177 °C. During the heating process, moisture in the samples vaporized from the oven to the condensing tube and was then collected in the receiving tube. Until the water volume no longer increased, it would be recorded. The water saturation could be calculated with measured pore volume on an alternative sample.

The samples were prepared as slices with approximately 1 cm^2 in size. These sample slices were treated with Ar ion milling in order to make their surfaces smooth and flat. Then the pore morphology, size and type can be observed by field emission scanning electron microscope (FE-SEM).

The powdered samples with grain size of 0.25 mm were dried and degassed at 378.15 K in a vacuum environment for more than 12 h. Then the prepared samples were exposed to nitrogen at constant temperature of 77 K. The adsorption isotherm was obtained with the increasing of the relative pressure from 0.00001 to 0.99. In contrast, the desorption isotherm was obtained with pressure reducing. Then the pore size distribution, pore volume, and pore surface area were then calculated using Barrett–Joyner–Halenda (BJH) and Brunauer–Emmett–Teller (BET) models from the adsorption–desorption isotherms.

Samples were ground into powder with 0.25 mm in diameter. The methane excess adsorption isotherms were measured using the gravimetric method (Wei et al., 2019). Main procedures were as follows. First, the mass and volume of the adsorption cell were measured by Archimedes method with nitrogen as fluid. Second, the samples were crushed into powders of 60–80 mesh, and these powder samples were dried and degassed at 110 °C for 8 h to remove moisture and impurity gas effectively. Third, after the powdered samples were placed in the adsorption cell, the mass and grain volume were determined with Helium as fluid. Finally, methane with purity of 99.99% was used as adsorbent, and the methane excess adsorption isotherms were measured at the temperature of 383.15 K and the pressure from 0.5 MPa to 30 MPa with 16 pressure points were set.

3.2. Supercritical Dubinin–Radushkevich model

According to the Gibbs adsorption model, the excess adsorption amount is measured by methane adsorption experiment. The absolute adsorption amount is related to the excess adsorption amount and can be calculated by Eq. (1) (Gasparik et al., 2012; Krooss et al., 2002).

$$n_{ex} = n_{ab} \cdot \left(1 - \frac{\rho_{free}}{\rho_{ad}}\right) \tag{1}$$

where n_{ex} is the excess adsorption amount, m^3/t rock; n_{ab} is the absolute adsorption amount, m^3/t rock; ρ_{free} is the density of free gas, kg/m^3; ρ_{ad} is the density of adsorbed gas, kg/m^3.

Methane occurs in the form of supercritical fluid in shale reservoirs (Hu et al., 2021c; Tang et al., 2019). The supercritical Dubinin–Radushkevich (SDR) model is usually used to fit the measured excess adsorption isotherms and obtain the absolute adsorption isotherms (Eq. (2), Rexer et al., 2013; Sakurovs et al., 2007). The SDR model was improved on the classical Dubinin–Radushkevich (DR) model that describes subcritical adsorption (Dubinin, 1989). Based on the pore filling mechanism, the SDR model takes the effect of shale pore structure on adsorption (Murata et al., 2001).

$$n_{ex} = n_0 \cdot \exp\left\{-D \cdot \left[\ln\left(\frac{\rho_{ad}}{\rho_{free}}\right) \cdot R \cdot T\right]^2\right\} \cdot \left(1 - \frac{\rho_{free}}{\rho_{ad}}\right) \tag{2}$$

where n_0 is the maximum absolute adsorption amount, m^3/t rock; D is an interaction constant related to pore structure, mol^2/kJ^2; R is the ideal gas constant, 8.314×10^{-3} kJ/(mol K); T is the temperature, K.

3.3. Control variable method

The control variable method was used to study the influence of a single geological factor on the occurrence state of shale gas. In other words, the implementation of this method is to regard a particular factor as a variable and quantitatively study the influence of the variable on the occurrence state of shale gas under the condition that other factors remain unchanged. Experimental groups I–V were set to investigate the effects of temperature, pressure, the coupling of temperature and pressure, pore structure, and organic matter content on the shale gas occurrence, respectively (Table 1). For example, experimental group I was set that except that temperature is the variable, other factors such as pressure, organic matter content, porosity, rock density, and water saturation are set to constant values. The values of these constants are the averages of the various parameters of the sample, respectively. Similarly, experimental group II takes pressure as the variable, whereas temperature and pressure are variables in experimental group III. Experimental group IV and V take TOC and porosity as the variables, respectively.

4. Results

4.1. Organic matter, mineral composition and lithofacies

The TOC contents of the Longmaxi shale samples are in the range of 1.70 wt%∼3.74 wt%, with an average of 2.72 wt%1u (Table 2). XRD analysis show that the Longmaxi shale samples are mainly consisted of clay minerals, Quartz and carbonates. The contents of clay minerals range from 34% to 51%, averaging 43.25%, mainly including illite and mixed illite/smectite. The

Table 1
Parameters of control variable experiments.

Experimental group	Temperature (K)	Pressure (MPa)	TOC (wt.%)	Porosity (%)	Shale density (g/cm^3)	Water saturature (%)
I	Variable	72	2.72	7.54	2.52	40.8
II	420	Variable	2.72	7.54	2.52	40.8
III	Variable	Variable	2.72	7.54	2.52	40.8
IV	420	72	Variable	7.54	2.52	40.8
V	420	72	2.72	Variable	2.52	40.8

Table 2
TOC and mineral compositions for the Longmaxi shale samples in the Weirong block, Sichuan Basin.

Samples	Depth (m)	TOC (wt.%)	Clay (%)	Quartz (%)	Feldspar (%)	Calcite (%)	Dolomite (%)	Pyrite (%)	Siderite (%)	Anhydrite (%)
1	3815.85	2.33	51	34	4	2	3	4	1	1
2	3827.69	2.33	34	29	2	16	16	2	1	0
3	3830	3.36	43	30	2	9	12	3	1	0
4	3832.4	3.74	39	37	2	8	10	3	1	0
5	3836.72	3.58	48	31	2	3	9	5	1	1
6	3837.82	3.03	42	42	3	2	5	4	1	1
7	3839.17	1.70	48	35	6	3	3	5	0	0
8	3840.96	1.71	41	28	4	6	17	2	1	1

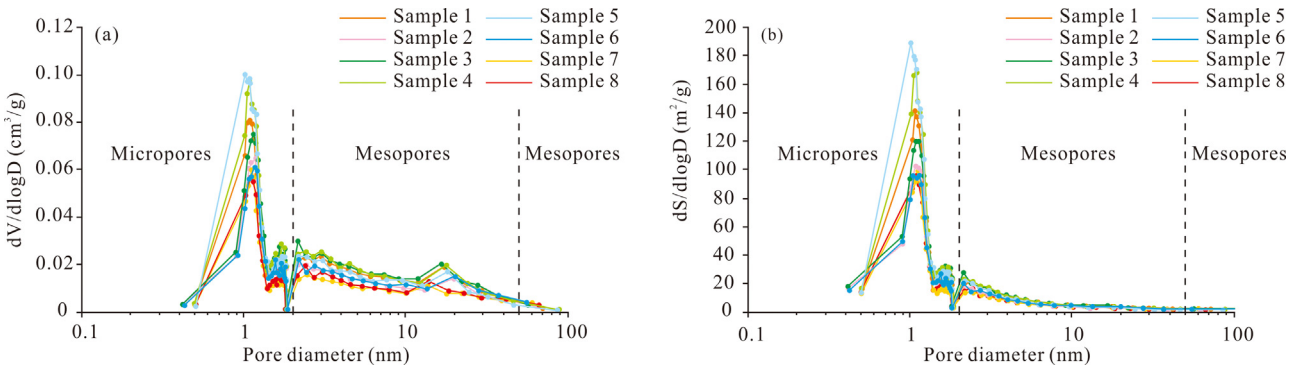

Fig. 5. Differential distribution of (a) pore volumes and (b) pore surface areas for the Longmaxi shale samples in the Weirong block, Sichuan Basin.

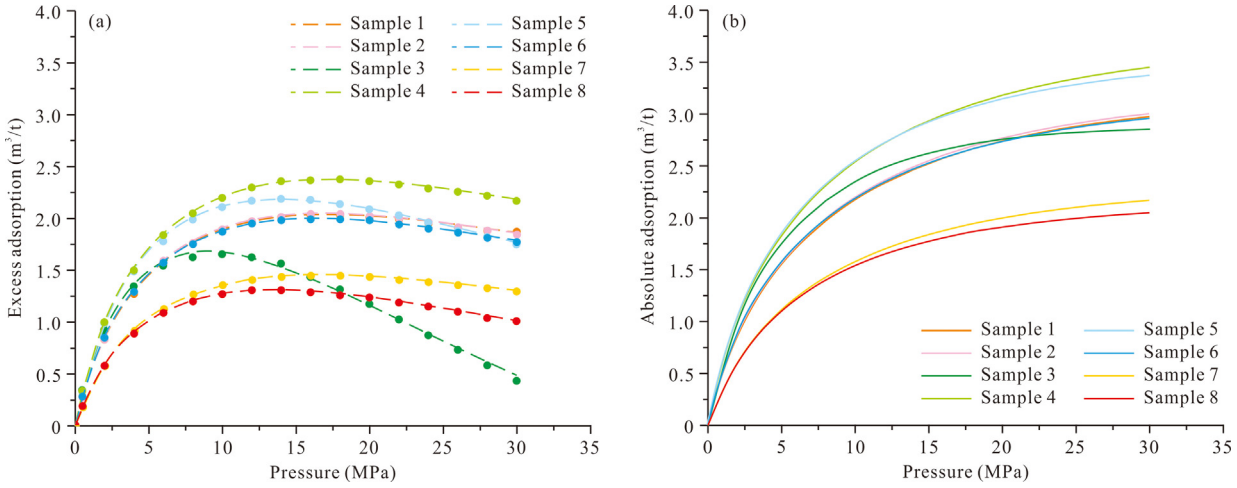

Fig. 6. Adsorption isotherms at 383.15 K for the Longmaxi shale samples in the Weirong block, Sichuan Basin. (a) Fitted excess adsorption isotherms using the SDR model. The color circles represent measured data, and the dotted lines represent the fitting curves; (b) Absolute adsorption isotherms calculated by the SDR model. (For interpretation of the references to color in this figure legend, the reader is referred to the web version of this article.)

quartz proportion range between 28% and 37%, averaging 33.25%. The carbonate contents range from 5%∼32%, with an average of 15.50%. Feldspars and pyrites have low percentages with their average contents both less than 5%. Combining the mineralogical compositions and TOC contents, the lithofacies can be identified. The Longmaxi shale samples are mainly organic-rich argillaceous, argillaceous siliceous and siliceous argillaceous (Fig. 2).

4.2. Pore structure characteristics

Based on the pore type classification of Loucks et al. (2012), the pore types in the Longmaxi shale samples are mainly mineral matrix pores and organic pores. The common mineral matrix pores in the shale samples are interparticle pores between quartz grains, intraplatelet pores within clay aggregates, and intercrystalline pores within pyrite frambodies. It was observed by

Table 3
Pore volumes and surface areas for the Longmaxi shale samples in the Weirong block, Sichuan Basin.

Sample	Pore volume (cm^3/g)				Pore surface area (m^2/g)				Porosity (%)	Average pore size (nm)
	Micropore	Mesopore	Macropore	Total	Micropore	Mesopore	Macropore	Total		
1	0.011	0.022	0.003	0.036	19.552	7.272	0.044	26.868	9.76	5.34
2	0.011	0.018	0.003	0.032	20.598	5.922	0.052	26.573	7.41	4.81
3	0.013	0.024	0.004	0.041	23.695	7.855	0.063	31.613	7.02	5.21
4	0.013	0.023	0.003	0.039	22.889	7.955	0.029	30.873	7.43	5.06
5	0.013	0.020	0.003	0.036	22.660	7.188	0.029	29.876	8.50	4.81
6	0.011	0.018	0.005	0.034	19.047	5.865	0.073	24.986	8.14	5.41
7	0.008	0.014	0.004	0.026	13.761	4.487	0.060	18.308	6.51	5.65
8	0.008	0.016	0.003	0.027	14.623	5.165	0.057	19.845	5.57	5.46
Average	0.011	0.019	0.004	0.034	19.603	6.464	0.051	26.118	7.54	5.22

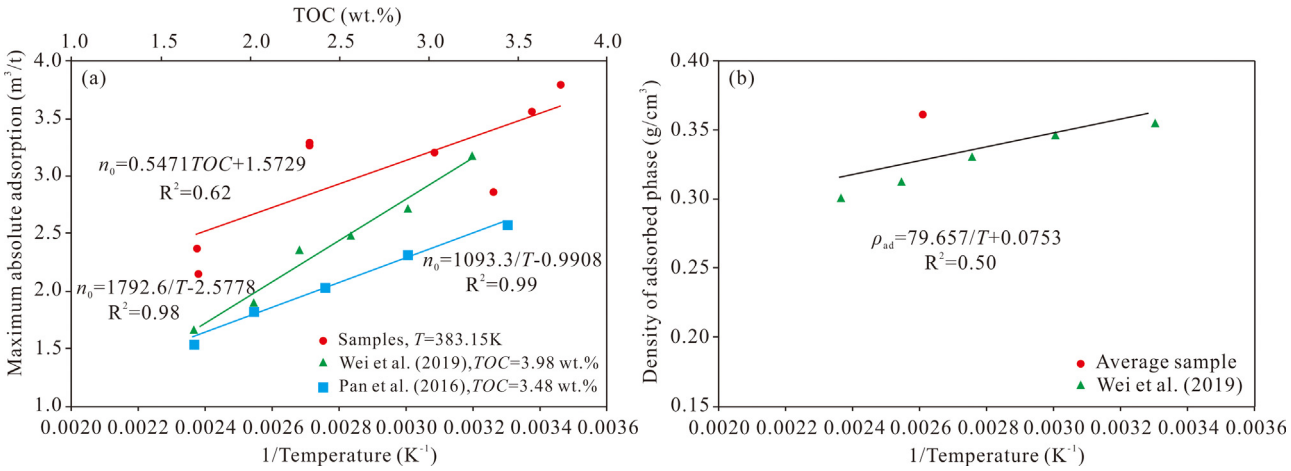

Fig. 7. Plots showing the relationships between the maximum absolute adsorption and the reciprocal of temperature, and TOC (a), between the density of adsorbed phase and the reciprocal of temperature (b) for the Longmaxi shale samples in the Weirong block, Sichuan Basin.

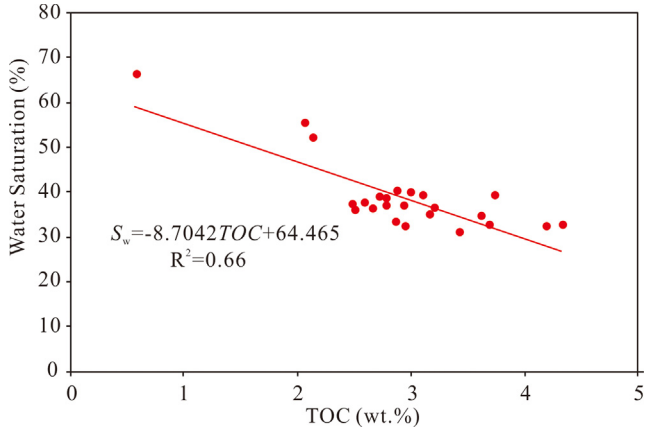

Fig. 8. Plots showing the relationships between the water saturation and TOC for the Longmaxi shale samples in the Weirong block, Sichuan Basin.

scanning electron microscope (SEM) that the interparticle pores between quartz grains and the intercrystalline pores within pyrite frambodies are generally macropores and mesopores. These pores are generally triangular and irregular. In contrast, the intraplatelet pores within clay aggregates are mainly mesopores and micropores of slit-like shape (Fig. 3a–c). The organic pores are more abundant than the mineral matrix pores since many mineral matrix pores are filled with organic matter (Fig. 3d). The organic pores are mainly near-circular and elliptical, and their size mainly ranges from 5 nm to 150 nm, with micropores and mesopores are most developed (Fig. 3e–i).

The results of porosity measurement show that the porosity of Longmaxi shale formation is mainly in the range of 5.57%–9.76%, with an average value of 7.54% (Table 3). According to the IUPAC classification (Sing et al., 1985), the shape of the nitrogen adsorption isotherms is type IV, and the hysteresis loops of the isotherms are similar to H2 and H3 types, indicating the samples are abundant with slit-like and 'ink bottle' pores (Fig. 4). The pore size distributions of the Longmaxi shale samples show multi-peak characteristics (Fig. 5). Pores in diameter of 0.6∼1.2 nm are most rich, followed by pores in diameter of 2.0∼3.5 nm, which shows that micropores (<2 nm) are most developed in the shale samples, the second is mesopores (2∼50 nm), and the last is macropores (>50 nm). The average pore size is approximately 5.22 nm. The total pore volumes of the shale samples vary from 0.027 to 0.041 cm^3/g, with an average of 0.034 cm^3/g (Table 3). Moreover, the average micropore, mesopore, and macropore volumes are 0.011 cm^3/g, 0.019 cm^3/g, and 0.004 cm^3/g, respectively. The pore volume of mesopores is the largest, micropores are the second, and macropores are the smallest. The total specific surface area of the shale samples ranges from 18.308 m^2/g to 31.613 m^2/g, with an average value of 26.118 m^2/g. The micropores, which have average specific surface area of 19.603 m^2/g, provide most of the surface areas of pores in shale. Followed are mesopores and macropores, with average specific surface areas of 6.464 m^2/g and 0.051 m^2/g, respectively.

4.3. Adsorbed gas, free gas and total gas contents

Based on the SDR model, the contents of adsorbed gas, free gas, and total gas in shale reservoirs can be calculated using Eqs. (3)–(6) (Ambrose et al., 2012; Gasparik et al., 2014; Sandoval et al., 2018). As shown in Fig. 6, the measured excess adsorption isotherms of eight shale samples are fitted well with

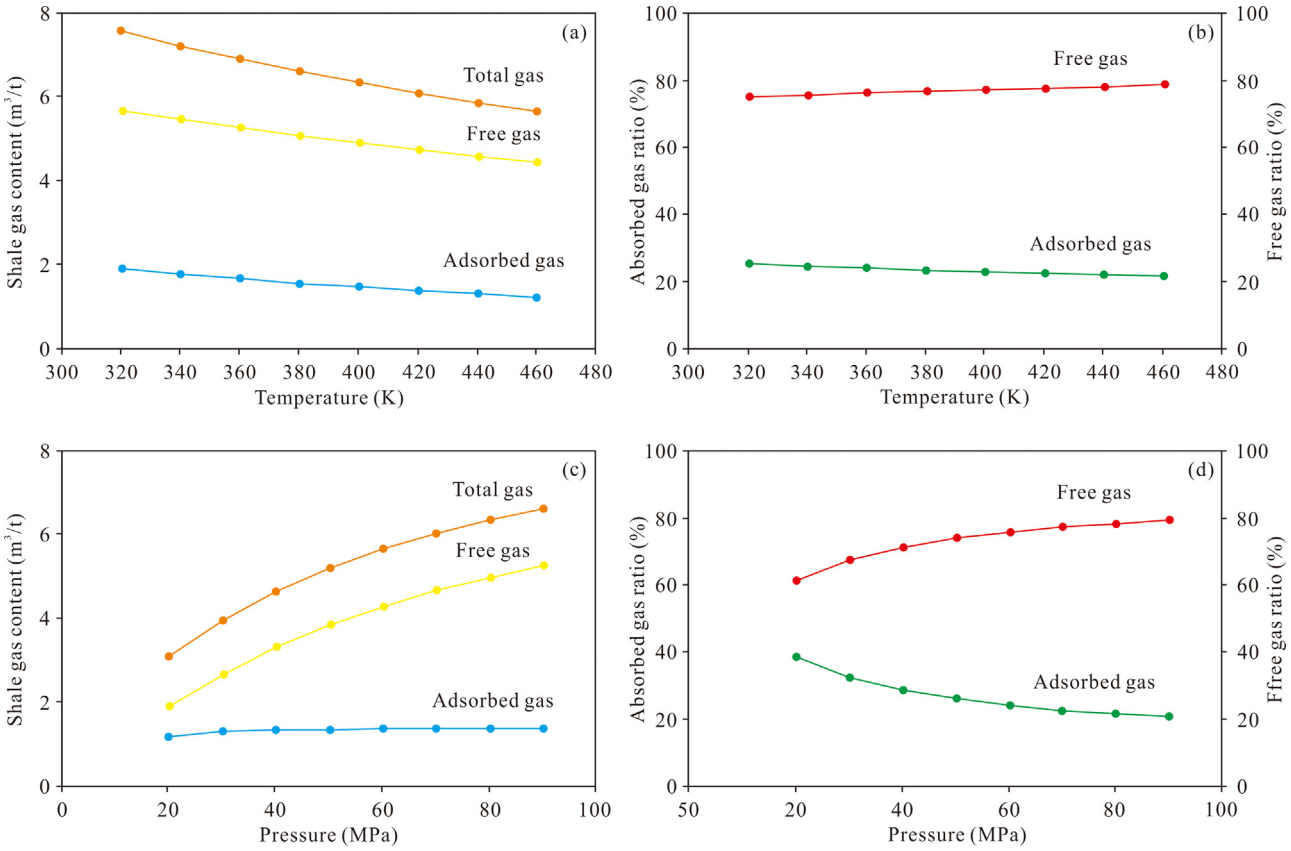

Fig. 9. Effect of temperature on adsorbed gas, free gas and total gas content under the pressure of 72 MPa (a); Effect of temperature on the proportion of adsorbed gas and free gas under the pressure of 72 MPa (b), Effect of pressure on adsorbed gas, free gas and total gas content under the temperature of 420 K (c); Effect of pressure on the proportion of adsorbed gas and free gas under the temperature of 420 K (d).

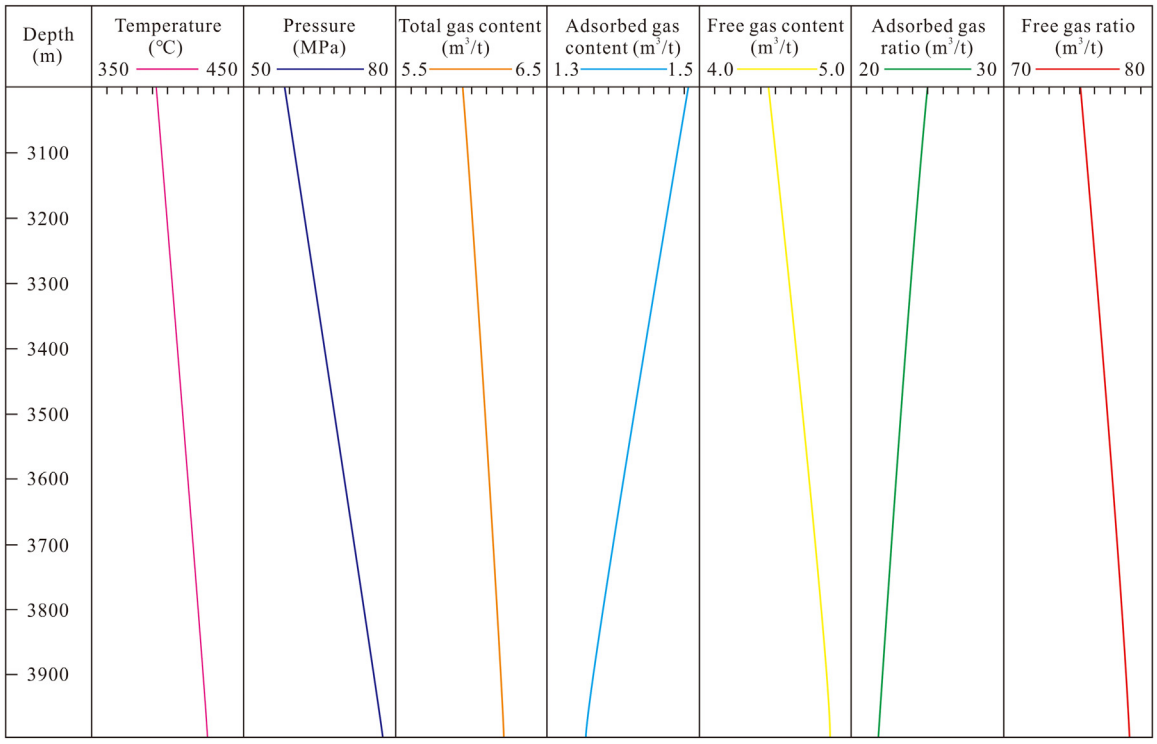

Fig. 10. Profile shows the coupling influence of temperature and pressure on the occurrence characteristics of shale gas. Based on the geothermal gradient (3.32 °C/100 m) and pressure coefficient (1.94) of the Weirong block, the variations of temperature and pressure at a depth of 3000–4000 m which corresponds to the depth range of the Longmaxi Formation are obtained.

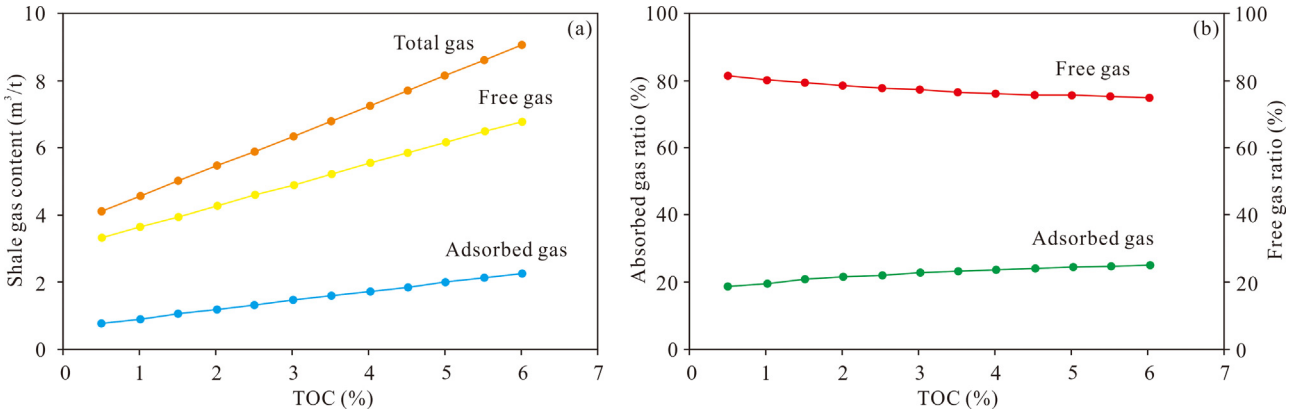

Fig. 11. Effect of TOC on adsorbed gas, free gas and total gas content (a); Effect of porosity on the proportion of adsorbed gas and free gas (b). The temperature and pressure corresponding to the middle depth of the Longmaxi Formation is 420 K and 72 MPa, respectively.

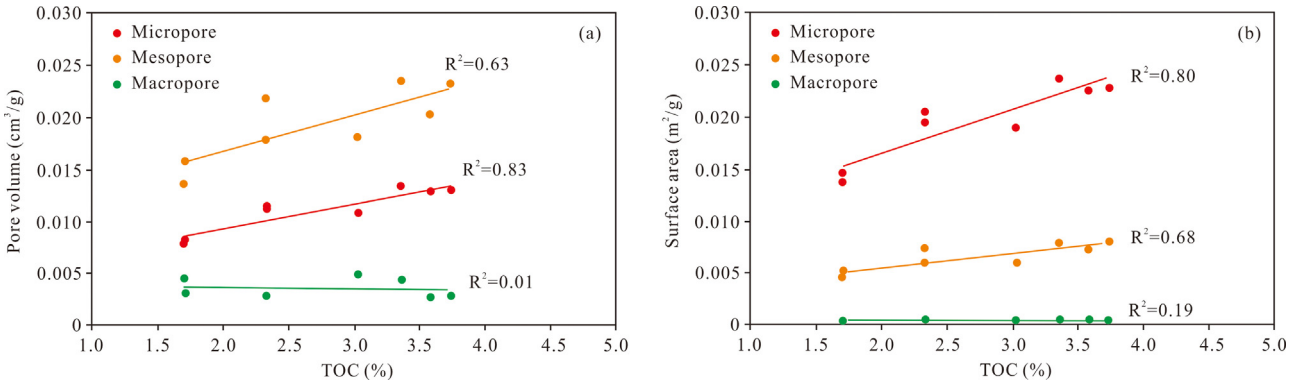

Fig. 12. Plots showing the relationships between pore volumes (a) and surface areas (b) of micropores, mesopores and macropores with TOC for the Longmaxi shale samples in the Weirong block, Sichuan Basin.

the SDR model. The excess and absolute adsorption isotherms show different shapes for all samples. The excess adsorbed gas content increases with pressure and then reduces with pressure increasing after reaching the maximum at 16∼18 MPa. At the same time, the absolute adsorbed gas amount rapidly increases and then slowly increases with pressure. Under experimental conditions, the free parameters (n_0, D, and ρ_{ad}) in Eq. (2) were obtained. Research shows that the n_0 is positively related to the TOC and negatively correlated with temperature (Pan et al., 2016; Weniger et al., 2010; Tian et al., 2016), the ρ_{ad} has a negative relationship with temperature (Li et al., 2017; Rexer et al., 2013; Wei et al., 2019), and the D is generally regarded as a constant (Rexer et al., 2014; White et al., 2005), with a value of 0.01059 mol^2/kJ^2 in this study. Because the methane isothermal adsorption experiment was carried out only at the temperature of 383.15 K, it is necessary to obtain the relationship between n_0, ρ_{ad}, and temperature through literature research. At 383.15 K, n_0 positively correlates with TOC (Fig. 7a). Pan et al. (2016) and Wei et al. (2019) proposed that when TOC content is constant, n_0 is positively correlated with the reciprocal of temperature and increases linearly with the increase of the reciprocal of temperature, with an average slope of 1142.95 (Fig. 7a). Based on the above results, the n_0 can be obtained by TOC and temperature (Eq. (7)), and the error is less than 10%. The relationship between ρ_{ad} and temperature is referred to by Wei et al. (2019), combined with the average value of ρ_{ad} under 383.15 K in this study, and the ρ_{ad} can be obtained by temperature based on Eq. (8) with an accuracy of about 85% (Fig. 7b).

Besides the above three parameters, other geological parameters, including T, P, ρ_s, φ, S_w and k_w, needed to be determined. The drilling results showed that the present geothermal gradient is 3.32 °C/100 m, and the fluid pressure coefficient, the ratio of pore pressure to hydrostatic pressure, is approximately 1.94 in the Weirong block. The ρ_s and φ are obtained from experiments. The S_w of the 25 shale samples from the Longmaxi Formation was obtained by core analysis. The S_w has a negative correlation with TOC, shown in Eq. (9) (Fig. 8). Then the situ S_w of eight shale samples can be calculated, ranging from 31.9%–49.7%, with an average of 40.8% (Table 4). Previous studies revealed that the methane adsorption amount decreased with increasing S_w until the critical moisture content (Merkel et al., 2016; Shabani et al., 2018). Yang et al. (2017) found that the amount of adsorbed gas of shale samples with water content at 75% relative humidity (RH) (equivalent S_w of 27%–67%) can be reduced by 39%–51%, compared with that of dry shale. Whitelaw et al. (2019) proposed that the adsorption capacity decreased by 27% after the shale samples were equilibrated at 50% RH. Li et al. (2021b) also found that 46%–72% of methane adsorption capacity of shale samples at 95% RH were lost. Since the Longmaxi shale samples for the methane adsorption experiment were dehydrated, the k_w is used to reflect the effect of moisture on gas adsorption and correct the adsorbed gas amount. Based on the high S_w characteristics of the shale samples, the k_w of this study is determined as 50%, which is consistent with that selected by Wei et al. (2019) in studying

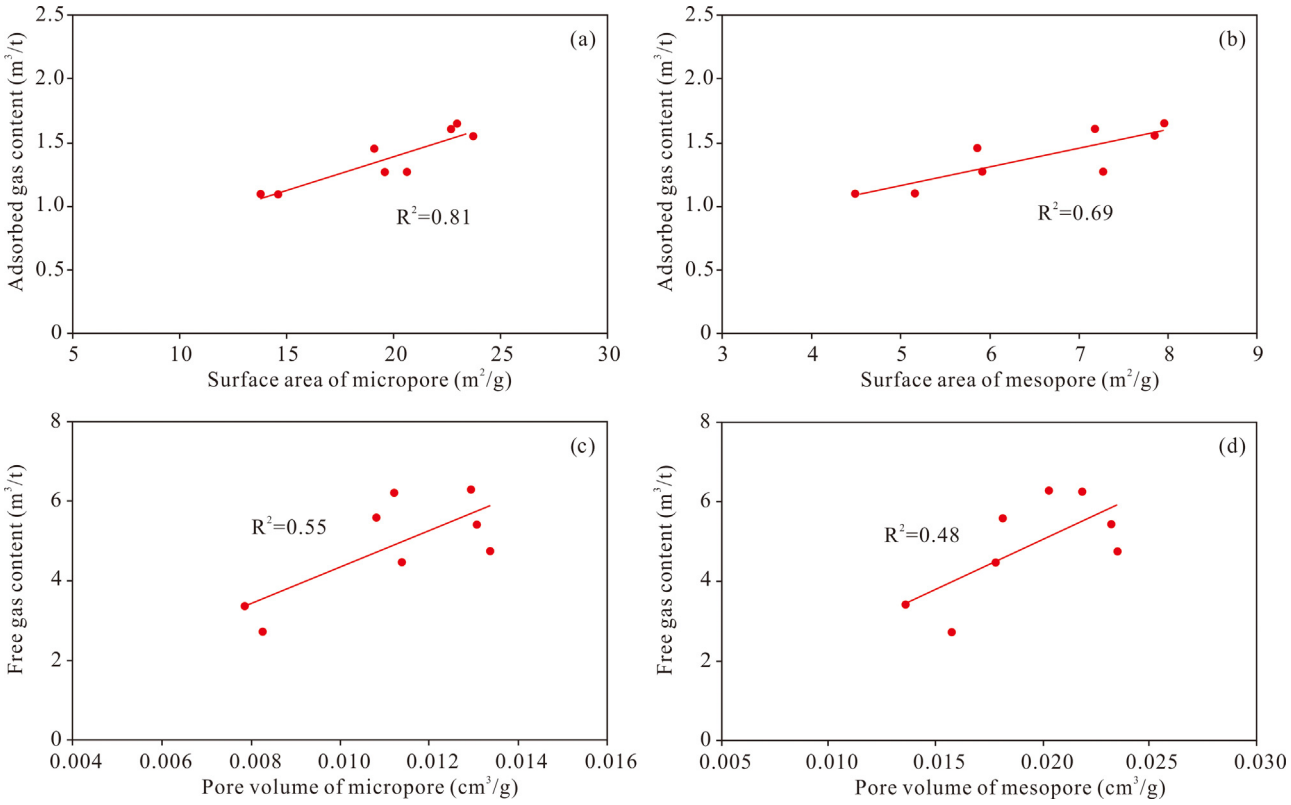

Fig. 13. Plots showing the relationships between adsorbed gas content and surface area of micropores (a), between adsorbed gas content and surface area of mesopores (b), between free gas content and pore volume of micropores (c), between free gas content and pore volume of mesopores (d) for the Longmaxi shale samples in the Weirong block, Sichuan Basin.

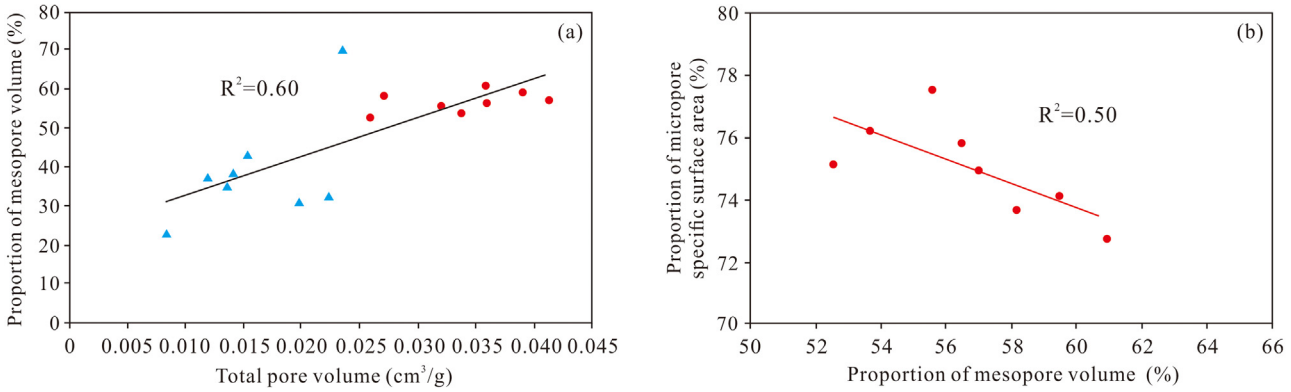

Fig. 14. The relationships between porosity and total pore volume (a), and between proportion of mesopores and total pore volume (b) for the Longmaxi shale samples. The dots represent the measured data in this study, while the triangles are collected data from Jiang et al. (2016).

adsorption capacity of the Longmaxi shale.

$$n_{ex}^{T,P} = n_0^{TOC,T} \cdot \exp\left\{-D \cdot \left[\ln\left(\frac{\rho_{ad}^{T}}{\rho_{free}^{T,P}}\right) \cdot R \cdot T\right]^2\right\} \cdot \left(1 - \frac{\rho_{free}^{T,P}}{\rho_{ad}^{T}}\right) \cdot k_w \quad (3)$$

$$n_{ab}^{T,P} = n_0^{TOC,T} \cdot \exp\left\{-D \cdot \left[\ln\left(\frac{\rho_{ad}^{T}}{\rho_{free}^{T,P}}\right) \cdot R \cdot T\right]^2\right\} \cdot k_w \quad (4)$$

$$n_{total}^{T,P} = n_{ex}^{T,P} + \frac{\varphi \cdot (1 - S_w)}{\rho_s} \cdot \frac{\rho_{free}^{T,P}}{\rho_{free}^{STP}} \quad (5)$$

$$n_{free}^{T,P} = n_{total}^{T,P} - n_{ab}^{T,P} \quad (6)$$

$$n_0^{TOC,T} = (0.5471 \cdot TOC + 1.5729) + (\frac{1}{T} - 0.0026) \times 1442.95 \quad (7)$$

$$\rho_{ad}^{T} = 79.657 \cdot \frac{1}{T} + 0.0753 \quad (8)$$

$$S_w = -8.7042 \cdot TOC + 64.465 \quad (9)$$

where $n_{ex}^{T,P}$, $n_{ab}^{T,P}$, $n_{free}^{T,P}$ and $n_{total}^{T,P}$ are the excess adsorbed gas amount, adsorbed gas amount, free gas amount and total gas amount under geological conditions, respectively, m^3/t rock; $n_0^{TOC,T}$ is the maximum absolute adsorption amount under geological conditions, m^3/t rock; ρ_{ad}^{T} is the adsorbed gas density under geological conditions, kg/m^3; $\rho_{free}^{T,P}$ is the free gas density under geological conditions which can be obtained from the

Table 4
Geological parameters and calculation results of adsorbed gas and free gas for the Longmaxi shale samples in the Weirong block, Sichuan Basin.

Samples	P (MPa)	T (K)	φ (%)	ρ_s (g/cm^3)	S_w (%)	Calculated n_0 (m^3/t)	Calculated ρ_{ad} (kg/m^3)	ρ_{free} (kg/m^3)	n_{ab} (m^3/t)	n_{free} (m^3/t)	n_{total} (m^3/t)	Free gas ratio (%)
3815.85	74.03	419.84	9.76	2.52	44.2	2.53	265.03	241.75	1.27	6.23	7.49	83
3827.69	74.26	420.23	7.41	2.51	44.2	2.53	264.86	241.94	1.26	4.48	5.74	78
3830	74.30	420.31	7.02	2.52	35.2	3.09	264.82	241.96	1.54	4.76	6.30	75
3832.4	74.35	420.39	7.43	2.49	31.9	3.30	264.79	242.01	1.65	5.44	7.09	77
3836.72	74.43	420.53	8.50	2.50	33.3	3.21	264.72	242.07	1.60	6.29	7.89	80
3837.82	74.45	420.57	8.14	2.49	38.1	2.91	264.70	242.09	1.45	5.59	7.04	79
3839.17	74.48	420.61	6.51	2.54	49.7	2.18	264.68	242.12	1.09	3.41	4.50	76
3840.96	74.51	420.67	5.57	2.58	49.6	2.19	264.66	242.14	1.09	2.72	3.82	71

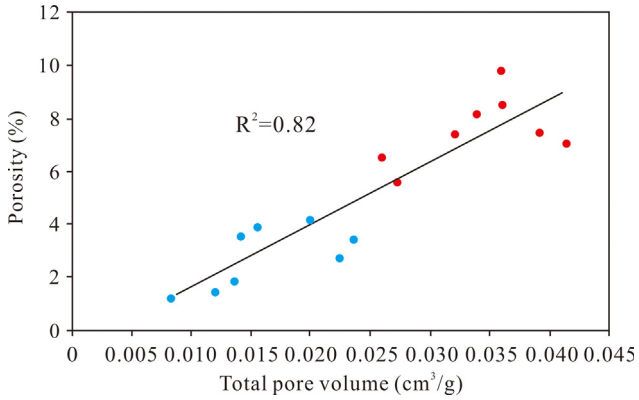

Fig. 15. The negative correlation between the proportion of mesopore volume and proportion of micropore specific surface area for the Longmaxi shale samples.

MIST website, kg/m^3; ρ_{free}^{STP} is the free gas density at standard temperature and pressure (273.15 K and 0.1 MPa), kg/m^3; ρ_s is the grain density of the Longmaxi shale, g/cm^3; k_w is the correction coefficient of adsorbed gas amount; generally the value of 50%; φ is the bulk porosity of the Longmaxi shale, %; S_w is the water saturation of the Longmaxi shale, %.

The geological parameters and the calculated gas contents are listed in Table 4. The adsorbed gas contents of the Longmaxi shale samples are 1.09∼1.65 m^3/t rock, with an average of 1.37 m^3/t rock. The free gas contents are in the range of 2.72∼6.29 m^3/t rock, with an average of 4.86 m^3/t rock. The total gas contents vary from 3.82 m^3/t rock to 7.89 m^3/t rock, with an average of 6.23 m^3/t rock. The ratios of free gas to total gas contents range from 71% to 83%, averaging a value of 77%.

5. Discussion

5.1. Influence of temperature and pressure on shale gas occurrence

Previous studies have shown that temperature and pressure are the two crucial influencing factors of shale gas occurrence state and content (Han et al., 2021; Hao et al., 2013; Miao et al., 2022; Wang et al., 2021). Temperature and pressure are inseparable, and they will affect shale gas content simultaneously during burial. This study focuses on the effect of temperature, pressure, and their coupling on shale gas occurrence by control variable experimental groups I–III (Table 1). The results show that temperature is negatively correlated with the contents of adsorbed gas and free gas (Fig. 9a). The effect of temperature on adsorbed gas content is more significant than that on free gas content. Thus, when the formation pressure is 72 MPa, the proportion of free gas relatively increases gradually with the increase of temperature, approximately by 0.03% on average for each increase of 1 K temperature. Different from the temperature, pressure is positively correlated with the content of adsorbed gas and free gas. The effect of pressure on free gas is significantly greater than that on adsorbed gas (Fig. 9b). When the formation temperature is 420 K, the proportion of free gas will increase by 0.25% on average if the pressure increases by 1 MPa. The variation profiles of the content and proportion of shale gas in different occurrence states with temperature and pressure during burial are shown in Fig. 10. The analysis indicates that the content and proportion of free gas and adsorbed gas change regularly under the coupling effect of temperature and pressure. With the increase of temperature and pressure, the adsorbed gas content decreases gradually. The free gas shows the opposite trend with a greater range, resulting in a rise in total gas content. Above all, pressure takes a larger effect on the occurrence state of shale gas than temperature. Therefore, the high-pressure conditions of the Longmaxi Formation are very conducive to the storage of free gas, resulting in the proportion of free gas in shale gas being much higher than that of adsorbed gas.

5.2. Influence of TOC on shale gas occurrence

Experimental group IV focused on the relationships of TOC contents and shale gas contents (Table 1). The results showed that TOC plays a positive role in the increase of adsorbed gas, free gas and total gas content (Fig. 11a). However, the content of free gas increases slower than the adsorbed gas content, causing the proportion of the free gas decreased with the increase of TOC (Fig. 11b). When the formation temperature and pressure are 420 K and 72 MPa, respectively, the proportion of free gas decreases by 1.2% on average for each increase of 1 wt% TOC. Therefore, the increase of organic matter content is conducive to promote the transformation of free gas to adsorbed gas. However, the TOC values of the Longmaxi shale mainly range from 1.70 wt% to 3.74 wt%, the content of organic matter is not enough to make the proportion of adsorbed gas exceed that of free gas.

The pore structure of organic matter of the Longmaxi shale determines that organic matter has a strong adsorption capacity for shale gas (Zhang et al., 2018). Micropores are mainly developed in the organic matter in the high-over mature stage (Qiu et al., 2021). In addition, TOC content has the best correlation with pore volume and specific surface area of micropores (Fig. 12). There are no apparent relationships between the TOC content and the pore volume and the specific surface area of macropores (Fig. 11). It indicates that micropores are primarily developed in organic matter, followed by mesopores. Organic matter is not the main contributor to the macropores. As discussed above, the adsorption capacity of micropores for shale gas is greater than that of mesopores and macropores. A large number of micropores in organic matter provide the site for adsorbed gas. Thus, the more abundant organic matter, the more development of micropores, and the larger proportion of adsorbed gas.

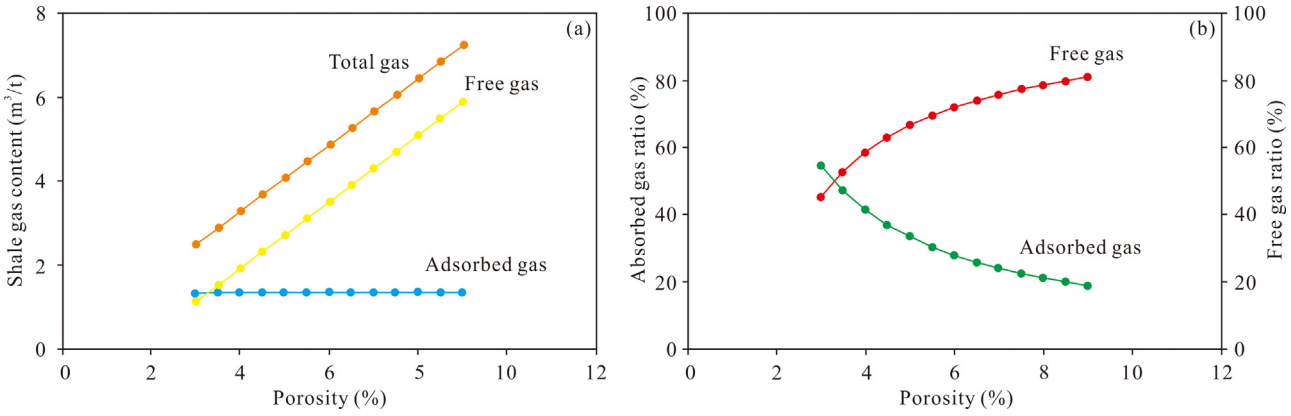

Fig. 16. Effect of porosity on adsorbed gas, free gas and total gas content (a); Effect of porosity on the proportion of adsorbed gas and free gas (b). The temperature and pressure corresponding to the middle depth of Longmaxi Formation is 420 K and 72 MPa, respectively.

5.3. Effect of pore structure on shale gas occurrence

The pores provide the primary space for shale gas storage in the shale reservoirs. Researches show that the pore structure can play an important role in shale gas occurrence state (Bakshi et al., 2018; He et al., 2018, 2019; Ross and Bustin, 2009; Slatt and O'Brien, 2011; Wang et al., 2016; Yang et al., 2016b; Zhu et al., 2018). This study discusses the influence of pore volume and specific surface area on the relative content of free gas and adsorbed gas. The adsorbed gas content has positive relationships with the specific surface area of micropores and mesopores (Fig. 13a–b). In contrast, the free gas content is positively correlated with the pore volume of micropores and mesopores (Fig. 13c–d), which agrees with the research results by Jiang et al. (2016). Thus the specific surface area of micropores and mesopores can affect the adsorbed gas content, and the free gas content is controlled by the pore volume of micropores and mesopores. As mentioned earlier, the specific surface areas of micropores account for approximately 75.1%. The proportions of the pore volumes of micropores and mesopores are 32.9% and 56.9%. It can be seen that the micropores have primary control on the adsorbed gas content, whereas both mesopores and micropores significantly control the free gas content.

Based on molecular mechanics, van der Waals force interaction exists between methane molecules, the main component of shale gas, and molecules of organic matter and minerals developing pores (Chalmers and Bustin, 2008). There is a distance limit between methane molecules and pore surfaces. Within the distance, methane molecules are adsorbed by van der Waals force. Beyond the distance, methane molecules are free without the action of van der Waals force. Thus, the adsorbed gas stores on the pore surface, and the free gas occupies the pore center (Fu et al., 2021; Li et al., 2020a; Qu et al., 2020; Xu and Prodanović, 2018). Especially, there is only adsorbed gas in the very tiny pores, while both adsorbed gas and free gas exist in the large pores (Chen et al., 2019b). It can be deduced that the proportion of adsorbed gas is absolutely dominant in tiny pores, and the proportion of free gas increases gradually with the enlargement of pores. Previous studies show that the critical pore size for free gas occurrence is approximately 1.8 nm (Chen et al., 2019b; Li et al., 2018a). It can be seen that the combination of mesopores and micropores determines the relative content of free gas and adsorbed gas to a certain extent. Free gas will account for a higher proportion when mesopores are much developed.

As can be seen from the above, mesopores are the main contributor to the total pore volume of the Longmaxi shale, followed by micropores. Further analysis shows a good positive correlation between the proportion of mesopore volume and the total pore volume (Fig. 14a). In contrast, the proportion of micropore specific surface area is inversely proportional to the proportion of mesopore volume (Fig. 14b). It can be inferred that with the increase of total pore volume, the proportion of mesopore volume generally increases, and the proportion of micropore specific surface area usually decreases. Above all, the total pore volume can reflect the relative development of micropores and mesopores. The mesopores of shale with large pore volume are more developed, and the development of micropores is relatively poor. Moreover, porosity is a parameter reflecting pore volume (Fig. 15). Porosity can also reveal the combination characteristics of micropores and mesopores in the Longmaxi shale to a certain extent. Thus, it can be deduced that high porosity indicates high pore volume of mesopores and much developed mesopores. The experimental group V studied the effect of porosity on the occurrence state of shale gas (Table 1). The results showed that the porosity change has little effect on the adsorbed gas content but dramatically effects the free gas content (Fig. 16a). With the increase of porosity, the proportion of free gas increases gradually, and the proportion of adsorbed gas decreases accordingly (Fig. 16b), which agrees with the findings of Chalmers and Bustin (2008) and Li et al. (2020b). When the porosity is greater than 3.3%, the proportion of free gas exceeds that of adsorbed gas; When the porosity is less than 3.3%, the opposite is true. Since the average porosity of Longmaxi shale reaches 7.54%, free gas is more enriched than adsorbed gas.

6. Conclusions

The Longmaxi shale in the Weirong block is deeply buried and high-over mature, mainly producing dry gas. Shale gas is primarily stored in micro and nanopores of shale in the form of free gas and adsorbed gas, of which free gas accounts for as much as 80%.

High pressure and large pore volume are the major factors causing a high proportion of free gas in the Longmaxi Formation. High pressure is beneficial to shale gas storage, and the positive influence on free gas is greater than that on adsorbed gas. The mesopores with absolute dominant pore volume are the primary place for free gas storage. The porosity of the Longmaxi shale is in the range of 5.57%–9.76%, with an average value of 7.54%, showing the extensive development of mesopores that provide sufficient storage space for free gas.

The study of shale gas occurrence characteristics of the Longmaxi Formation in the Weiyuan area provides theoretical guidance for predicting shale gas favorable areas in this area. Selecting the area with relatively high formation pressure and relatively high porosity as the important target of shale gas exploration

in the Longmaxi Formation is suggested. At the same time, this study also lays a foundation for the study of shale gas occurrence characteristics in other regions at home and abroad.

CRediT authorship contribution statement

Min Li: Conceptualization, Writing – original draft. **Xiongqi Pang:** Supervision, Funding acquisition. **Liang Xiong:** Resources, Data curation. **Tao Hu:** Validation, Methodology. **Di Chen:** Writing – review & editing. **Zhen Zhao:** Visualization. **Shasha Hui:** Investigation. **Yang Liu:** Investigation. **Siyu Zhang:** Software.

Declaration of competing interest

The authors declare that they have no known competing financial interests or personal relationships that could have appeared to influence the work reported in this paper.

Acknowledgments

This work was supported by the National Natural Science Foundation of China-Joint Fund Project [grant number U19B6003-02]. We thank SINOPEC Southwest Branch Company for providing essential data. Special thanks are given to the reviewers for their careful work and constructive comments.

References

Ambrose, R., Hartman, R., Diaz-Campos, M., Akkutlu, I.Y., Sondergeld, C., 2012. Shale gas-in-place calculations Part I: New pore-scaleconsiderations. SPE J. 17, 219–229.

Bakshi, T., Prusty, B.K., Pathak, K., Pal, S.K., 2018. Pore characteristics of damodar valley shale and their effect on gas storage potential. J. Pet. Sci. Eng. 162, 725–735.

Cao, T.T., Song, Z.J., Wang, S.B., Cao, X.X., Li, Y., Xia, J., 2015. Characterizing the pore structure in the silurian and permian shales of the Sichuan Basin, China. Mar. Pet. Geol. 61, 140–150.

Cao, X.J., Wang, M.G., Kang, J., Wang, S.H., Liang, Y., 2020. Fracturing technologies of deep shale gas horizontal wells in the Weirong Block, southern Sichuan Basin. Nat. Gas. Ind. B 7, 64–70.

Chalmers, G.R.L., Bustin, R.M., 2008. Lower cretaceous gas shales in northeastern British Columbia, Part I: geological controls on methane sorption capacity. Bull. Can. Petrol. Geol. 56, 1–21.

Chen, L., Jiang, Z.X., Liu, Q.X., Jiang, S., Liu, K.Y., Tan, J.Q., Gao, F.L., 2019a. Mechanism of shale gas occurrence: Insights from comparative study on pore structures of marine and lacustrine shales. Mar. Pet. Geol. 104, 200–216.

Chen, G.H., Lu, S.F., Liu, K.Y., Xue, Q.Z., Xu, C.X., Tian, S.S., Li, J.B., Zhang, Y.Y., Tong, M.S., Pang, X.T., Ni, B.W., Lu, S.D., Qi, Q.P., 2019b. Investigation of pore size effects on adsorption behavior of shale gas. Mar. Pet. Geol. 109, 1–8.

Curtis, J.B., 2002. Fractured shale-gas systems. AAPG Bull. 86 (11), 1921–1938.

Dai, J.X., Zou, C.N., Liao, S.M., Dong, D.Z., Ni, Y.Y., Huang, J.L., Wu, W., Gong, D.Y., Huang, S.P., Hu, G.Y., 2014. Geochemistry of the extremely high thermal maturity Longmaxi shale gas, southern Sichuan Basin. Org. Geochem. 74, 3–12.

Dubinin, M.M., 1989. Fundamentals of the theory of adsorption in micropores of carbon adsorbents: characteristics of their adsorption properties and microporous structures. Carbon 27, 457–467.

Etminan, S.R., Javadpour, F., Maini, B.B., Chen, Z.X., 2014. Measurement of gas storage processes in shale and of the molecular diffusion coefficient in kerogen. Int. J. Coal Geol. 123, 10–19.

Fu, X.X., Zhao, C.P., Lun, Z.M., Wang, H.T., Wang, M., Zhang, D.F., 2021. Influences of controlled microwave field radiation on pore structure, surface chemistry and adsorption capability of gas-bearing shales. Mar. Pet. Geol. 130, 105134.

Gasparik, M., Bertier, P., Gensterblum, Y., Ghanizadeh, A., Krooss, B.M., Littke, R., 2014. Geological controls on the methane storage capacity in organic-rich shales. Int. J. Coal Geol. 123 (2), 34–51.

Gasparik, M., Ghanizadeh, A., Bertier, P., Gensterblum, Y., Bouw, S., Krooss, B.M., 2012. High-pressuremethane sorption isotherms of black shales from the Netherlands. Energy Fuels 26, 4995–5004.

Gou, Q.Y., Xu, S., Hao, F., Shu, Z., Zhang, Z.Y., 2021. Making sense of micro-fractures to the Longmaxi shale reservoir quality in the Jiaoshiba area, Sichuan Basin, China: Implications for the accumulation of shale gas. J. Nat. Gas Sci. Eng. 94, 104107.

Guo, F.G., Wang, S., Feng, Q.H., Yao, X.Y., Xue, Q.Z., Li, X.F., 2020. Adsorption and absorption of supercritical methane within shale kerogen slit. J. Mol. Liq. 320, 114364.

Han, W.C., Li, A.I., Memon, A., Min, M., 2021. Synergetic effect of water, temperature, and pressure on methane adsorption in shale gas reservoirs. ACS Omega 6, 2215–2229.

Hao, F., Zou, H.Y., Lu, Y.C., 2013. Mechanisms of shale gas storage: Implications for shale gas exploration in China. AAPG Bull. 97 (8), 1325–1346.

He, Q., Dong, T., He, S., Zhai, G.Y., 2019. Methane adsorption capacity of marine-continental transitional facies shales: the case study of the upper permian longtan formation, northern Guizhou Province, Southwest China. J. Pet. Sci. Eng. 183, 106406.

He, J.L., Wang, J., Yu, Q., Liu, W., Ge, X.Y., Yang, P., Wang, Z.J., Lu, J.Z., 2018. Pore structure of shale and its effects on gas storage and transmission capacity in well HD-1 eastern Sichuan Basin, China. Fuel 226, 709–720.

Hou, L.H., Luo, X., Yu, Z.C., Wu, S.T., Zhao, Z.Y., Lin, S.H., 2021. Key factors controlling the occurrence of shale oil and gas in the Eagle Ford Shale, the Gulf Coast Basin: Models for sweet spot identification. J. Nat. Gas Sci. Eng. 94, 104063.

Hu, H.Y., Hao, F., Guo, X.S., Yi, J.Z., Shu, Z.G., Bao, H.Y., Zhu, X.Y., 2019. Effect of lithofacies on the pore system of over-mature Longmaxi shale in the Jiaoshiba area, Sichuan Basin, China. Mar. Pet. Geol. 109, 886–898.

Hu, T., Pang, X.Q., Jiang, F.J., Wang, Q.F., Liu, X.H., Wang, Z., Jiang, S., Wu, G.Y., Li, C.J., Xu, T.W., Li, M.W., Yu, J.W., Zhang, C.X., 2021a. Movable oil content evaluation of lacustrine organic-rich shales: Methods and a novel quantitative evaluation model. Earth Sci. Rev. 214, 103545.

Hu, T., Pang, X.Q., Jiang, F.J., Wang, Q.F., Wu, G.Y., Liu, X.H., Jiang, S., Li, C.R., Xu, T.W., Chen, Y.Y., 2021b. Key factors controlling shale oil enrichment in saline lacustrine rift basin: implications from two shale oil wells in Dongpu Depression, Bohai Bay Basin. Pet. Sci. 18, 687–711.

Hu, R.N., Wang, W.H., Tan, J.Q., Chen, L., Dick, J., He, G.M., 2021c. Mechanisms of shale gas adsorption: Insights from a comparative study on a thermodynamic investigation of microfossil-rich shale and non-microfossil shale. Chem. Eng. J. 411, 128463.

Ji, L.M., Zhang, T.W., Milliken, K.L., Qu, J.L., Zhang, X.L., 2012. Experimental investigation of main controls to methane adsorption in clay-rich rocks. Appl. Geochem. 27, 2533–2545.

Jiang, Z.X., Tang, X.L., Li, Z., Huang, H.X., Yang, P.P., Yang, X., Li, W.B., Hao, J., 2016. The whole-aperture pore structure characteristics and its effect on gas content of the Longmaxi Formation shale in the southeastern Sichuan basin. Earth Sci. Front. 23 (2), 126–134, (in Chinese with English abstract).

Krooss, B.M., van Bergen, F., Gensterblum, Y., Siemons, N., Pagnier, H.J.M., David, P., 2002. High pressure CH4 and carbon dioxide adsorption on dry and moisture equilibrated Pennsylvanian coals. Int. J. Coal Geol. 51, 69–92.

Li, Y.R., Hu, Z.M., Cai, C.H., Liu, X.G., Duan, X.G., Chang, J., Li, Y.L., Mu, Y., Zhang, Q.X., Zeng, S.T., Guo, J.S., 2021a. Evaluation method of water saturation in shale: A comprehensive review. Mar. Pet. Geol. 128, 105017.

Li, Y.X., Hu, Z.M., Liu, X.G., Gao, S.S., Duan, X.G., Chang, J., Wu, J.F., 2018a. Insights into interactions and microscopic behavior of shale gas in organic-rich nano-slits by molecular simulation. J. Nat. Gas Sci. Eng. 59, 309–325.

Li, J.Q., Lu, S.F., Zhang, P.F., Cai, J.C., Li, W.B., Wang, S.Y., Feng, W.J., 2020a. Estimation of gas-in-place content in coal and shale reservoirs: a process analysis method and its preliminary application. Fuel 259, 116266.

Li, Q.W., Pang, X.Q., Tang, L., Chen, G., Shao, X.H., Jia, N., 2018b. Occurrence features and gas content analysis of marine and continental shales: A comparative study of Longmaxi Formation and Yanchang Formation. J. Nat. Gas Sci. Eng. 56, 504–522.

Li, W., Stevens, L.A., Uguna, C.N., Vane, C.H., Meredith, W., Tang, L., Li, Q.W., Snape, C.E., 2021b. Comparison of the impact of moisture on methane adsorption and nanoporosity for over mature shales and their kerogens. Int. J. Coal Geol. 237, 103705.

Li, T.F., Tian, H., Xiao, X.M., Cheng, P., Zhou, Q., Wei, Q., 2017. Geochemical characterization and methane adsorption capacity of overmature organic-rich Lower Cambrian shales in northeast Guizhou region, southwest China. Mar. Pet. Geol. 86, 858–873.

Li, Z., Zhang, J.C., Gong, D.J., Tan, J.Q., Liu, Y., Wang, D.S., Li, P., Tong, Z.Z., Niu, J.L., 2020b. Gas-bearing property of the Lower Cambrian Niutitang Formation shale and its influencing factors: A case study from the Cengong block, northern Guizhou Province, South China. Mar. Pet. Geol. 120, 104556.

Loucks, R.G., Reed, R.M., Ruppel, S.C., Hammes, U., 2012. Spectrum of pore types and networks in mudrocks and a descriptive classification for matrix-related mudrock pores. AAPG Bull. 96 (6), 1071–1098.

Ma, Y.Q., Fan, M.J., Lu, Y.C., Guo, X.S., Hu, H.Y., Chen, L., 2016. Geochemistry and sedimentology of the lower silurian longmaxi mudstone in southwestern China: Implications for depositional controls on organic matter accumulation. Mar. Pet. Geol. 75, 291–309.

Ma, X.H., Wang, H.Y., Zhou, S.W., Shi, Z.S., Zhang, L.F., 2021. Deep shale gas in China: Geological characteristics and development strategies. Energy Rep. 7, 1903–1914.

Merkel, A., Fink, R., Littke, R., 2016. High pressure methane sorption characteristics of lacustrine shales from the Midland Valley Basin, Scotland. Fuel 182, 361–372.

Miao, F., Wu, D., Liu, X.Y., Xiao, X.C., Zhai, W.B., Geng, Y.Y., 2022. Methane adsorption on shale under in situ conditions: Gas-in-place estimation considering in situ stress. Fuel 308, 121991.

Montgomery, S.L., Jarvie, D.M., Bowker, K.A., Pallastro, R.M., 2005. Mississippian Barnett Shale, Fort Worth basin, north-central Texas: gas-shale play with multitrillion cubic foot potential. AAPG Bull. 89, 155–175.

Murata, K., El-Merraoui, M., Kaneko, K., 2001. A new determination method of absolute adsorption isotherm of supercritical gases under high pressure with a special relevance to density-functional theory study. J. Chem. Phys. 114, 4196–4205.

Nie, H.K., Chen, Q., Zhang, G.R., Sun, C.X., Wang, P.W., Lu, Z.Y., 2021. An overview of the characteristic of typical Wufeng-Longmaxi shale gas fields in the Sichuan Basin, China. Nat. Gas. Ind. B 8, 217–230.

Nie, H.K., He, Z.L., Wang, R.Y., Zhang, G.R., Chen, Q., Li, D.H., Lu, Z.Y., Sun, C.X., 2020. Temperature and origin of fluid inclusions in shale veins of Wufeng-Longmaxi Formations, Sichuan Basin, south China: Implications for shale gas preservation and enrichment. J. Pet. Sci. Eng. 193, 107329.

Pan, L., Xiao, X.M., Tian, H., Zhou, Q., Cheng, P., 2016. Geological models of gas in place of the Longmaxi shale in Southeast Chongqing, South China. Mar. Pet. Geol. 73, 433–444.

Qiu, H.Y., Jiang, Z.X., Liu, Z.J., Chang, J.Q., Su, Z.F., Yang, Z.W., Zhou, W., 2021. Difference in pore structure characteristics between condensate and dry shale gas reservoirs: Insights from the pore contribution of different matrix components. J. Nat. Gas Sci. Eng. 96, 104283.

Qu, Z.G., Yin, Y., Wang, H., Zhang, J.F., 2020. Pore-scale investigation on coupled diffusion mechanisms of free and adsorbed gases in nanoporous organic matter. Fuel 260, 116423.

Rexer, T.F.T., Benham, M.J., Aplin, A.C., Thomas, K.M., 2013. Methane adsorption on shale under simulated geological temperature and pressure conditions. Energy Fuels 27, 3099–3109.

Rexer, T.F.T., Mathia, E.J., Aplin, A.C., Thomas, K.M., 2014. High-pressure methane adsorption and characterization of pores in Posidonia Shales and isolated kerogens. Energy Fuels 28 (5), 2886–2901.

Ross, D.J.K., Bustin, R.M., 2009. The importance of shale composition and pore structure upon gas storage potential of shale gas reservoirs. Mar. Pet. Geol. 26 (6), 916–927.

Sakurovs, R., Day, S., Weir, S., Duffy, G., 2007. Application of a modified Dubinin-Radushkevich equation to adsorption of gases by coals under supercritical conditions. Energy Fuels 21, 992–997.

Sandoval, D.R., Yan, W., Michelsen, M.L., Stenby, E.H., 2018. Modeling of shale gas adsorption and its influence on phase equilibrium. Ind. Eng. Chem. Res. 57, 5736–5747.

Shabani, M., Moallemi, S.A., Krooss, B.M., Amann-Hildenbrand, A., Zamani-Pozveh, Z., Ghalavand, H., Littke, R., 2018. Methane sorption and storage characteristics of organic-rich carbonaceous rocks, Lurestan province, southwest Iran. Int. J. Coal Geol. 186, 51–64.

Sing, K.S., Everett, D.H., Haul, R.A.W., Moscou, L., Pierotti, R.A., Rouquerol, J., Siemieniewsha, T., 1985. Reporting physisorption data for gas/solid systems with special reference to the determination of surface area and porosity. Pure Appl. Chem. 57, 603–619.

Slatt, R.G., O'Brien, N.R., 2011. Pore types in the Barnett and Woodford gas shales: contribution to understanding gas storage and migration pathways in fine-grained rocks. AAPG Bull. 95, 2017–2030.

Tang, X., Ripepi, N., Rigby, S., Mokaya, R., Gilliland, E., 2019. New perspectives on supercritical methane adsorption in shales and associated thermodynamics. J. Ind. Eng. Chem. 78, 186–197.

Tang, J.M., Xu, T.J., Cheng, B.J., Shen, J., Yu, Q., 2021. Sweet-spot prediction and aided design for drilling engineering: Application to deep shale gas reservoirs in Sichuan Basin. Geophys. Prospect. Pet. 60 (3), 479–487, (in Chinese with English abstract).

Tian, H., Li, T.F., Zhang, T.W., Xiao, X.M., 2016. Characterization of methane adsorption on overmature Lower Silurian–Upper Ordovician shales in sichuan basin, southwest China: Experimental results and geological implications. Int. J. Coal Geol. 156, 36–49.

Wang, K., Ren, H., Wang, Z., Ma, S., Wei, J., Ke, W., Guo, Y., 2021. Kinetic characteristics of CH4 adsorption on coals under variable temperature–pressure coupling interaction. Nat. Resour. Res. http://dx.doi.org/10.1007/s11053-021-09965-8.

Wang, Y., Zhu, Y.M., Liu, S.M., Zhang, R., 2016. Pore characterization and its impact on methane adsorption capacity for organic-rich marine shales. Fuel 181, 227–237.

Wei, S.L., He, S., Pan, Z.J., Guo, X.W., Yang, R., Dong, T., Yang, W., Gao, J., 2019. Models of shale gas storage capacity during burial and uplift: Application to Wufeng-Longmaxi shales in the fuling shale gas field. Mar. Pet. Geol. 109, 233–244.

Weniger, P., Kalkreuth, W., Busch, A., Krooss, B.M., 2010. High-pressure methane and carbon dioxide sorption on coal and shale samples from the Paraná Basin, Brazil. Int. J. Coal Geol. 84, 190–205.

White, C.M., Smith, D.H., Jones, K.L., Goodman, A.L., Jikich, S.A., LaCount, R.B., DuBose, S.B., Ozdemir, E., Morsi, B.I., Schroeder, K.T., 2005. Sequestration of carbon dioxide in coal with enhanced coalbed methane recovery-a review. Energy Fuels 19 (3), 659–724.

Whitelaw, P., Uguna, C.N., Stevens, L.A., Meredith, W., Snape, C.E., Vane, C.H., Moss-Hayes, V., Carr, A.D., 2019. Shale gas reserve evaluation by laboratory pyrolysis and gas holding capacity consistent with field data. Nat. Commun. 10, 1–10.

Xiong, L., 2019. Characteristics and significance of sedimentary facies of Wufeng-Longmaxi formation shale in Weirong Shale Gas Field, southern Sichuan Basin. Pet. Geol. Exp. 41 (3), 326–332, (in Chinese with English abstract).

Xu, R., Prodanović, M., 2018. Effect of pore geometry on nitrogen sorption isotherms interpretation: a pore network modeling study. Fuel 225, 243–255.

Yang, Y.M., Chen, Y.L., Liu, S.Y., Deng, B., Xu, H., Chen, L.Q., Li, D.Y., Yin, Y.Z., Li, Y., 2021. Status, potential and prospect of shale gas exploration and development in the Sichuan Basin and its periphery. Nat. Gas. Ind. B 41 (1), 42–58.

Yang, R., He, S., Wang, X., Hu, Q.H., Hu, D.F., Yi, J.Z., 2016a. Paleo-ocean redox environments of the upper ordovician Wufeng and the first member in lower Silurian Longmaxi formations in the Jiaoshiba area, Sichuan Basin. Can. J. Earth Sci. 53, 426–440.

Yang, F., Ning, Z.F., Wang, Q., Zhang, R., Krooss, B.M., 2016b. Pore structure characteristics of lower Silurian shales in the southern Sichuan Basin, China: insights to pore development and gas storage mechanism. Int. J. Coal Geol. 156, 12–24.

Yang, F., Xie, C.J., Ning, Z.F., Krooss, B.M., 2017. High-pressure methane sorption on dry and moisture-equilibrated shales. Energy Fuels 31, 482–492.

Yuan, Y.J., Rezaee, R., Yu, H.Y., Zou, J., Liu, K.Q., Zhang, Y.H., 2021. Compositional controls on nanopore structure in different shale lithofacies: A comparison with pure clays and isolated kerogens. Fuel 303, 121079.

Zhang, L.C., Li, B., Jiang, S., Xiao, D.S., Lu, S.F., Zhang, Y.Y., 2018. Heterogeneity characterization of the lower Silurian Longmaxi marine shale in the Pengshui area, South China. Int. J. Coal Geol. 195, 250–266.

Zhou, Q., Xiao, X.M., Tian, H., Pan, L., 2014. Modeling free gas content of the Lower Paleozoic shales in the weiyuan area of the Sichuan Basin, China. Mar. Pet. Geol. 56, 87–96.

Zhu, H.J., Ju, Y.W., Huang, C., Chen, F.W., Chen, B.Z., Yu, K., 2020. Microcosmic gas adsorption mechanism on clay-organic nanocomposites in a marine shale. Energy 117256.

Zhu, H.H., Zhang, T.S., Liang, X., Zhang, Z., Zhang, L., 2018. Insight into the pore structure of Wufeng-Longmaxi black shales in the south Sichuan Basin, China. J. Pet. Sci. Eng. 171, 1279–1291.

Zou, C.N., Yang, Z., Sun, S.S., Zhao, Q., Bai, W.H., Liu, H.L., Pan, S.Q., Wu, S.T., Yuan, Y.L., 2020. Exploring petroleum inside source kitchen: Shale oil and gas in Sichuan Basin. Sci. China Earth Sci. 63, 934–953, (in Chinese with English abstract).